II. Technical Report

A. SUMMARY

We have been studying the widely discussed dynamic weakening mechanism termed *thermal pore-fluid pressurization*. There are many theoretical and numerical studies of thermal pressurization [*Andrews*, 2002; *Lachenbruch*, 1980; *Lee and Delaney*, 1987; *Mase and Smith*, 1985; 1987; *Noda*, 2008; *Noda and Shimamoto*, 2005; *Rempel and Rice*, 2006; *Rice*, 2006; *Rice and Cocco*, 2007; *Sibson*, 1973] and it is increasingly used in dynamic rupture and earthquake nucleation models [*Bizzarri and Cocco*, 2006a; b; *Lapusta and Rice*, 2004a; b; *Noda et al.*, 2009; *Noda and Lapusta*, 2010; *Rice et al.*, 2010; *Schmitt and Segall*, 2009; *Segall and Rice*, 2006]. Our experiment studies of thermal pressurization are the most definitive ones yet obtained.

This project is a continuation of the work funded in our current proposal of the same title. With SCEC 2017 funding we continued experiments to further investigate fault-weakening via thermal pore-fluid pressurization. Part of our emphasis has been on trying to understand the role that fault-roughness-induced dilatancy may play in defeating this weakening mechanism on natural faults. Part of it has also been to make more precise measurement of both the permeability and the storage capacity of our samples. These data are needed to determine the fluid diffusivity, the critical parameter needed to quantitatively understand thermal pressurization.

B. DETAILS

As stated earlier, the purpose of this project is both to demonstrate that we can reproducibly create thermal pressurization weakening and to determine whether or not dilatancy due to sliding on initially mated faults with realistic roughness defeats the thermal pressurization. In the past, some, but not all, of the samples that we expected to weaken due to thermal pressurization actually did so. Because of this, during this year we have focused our experiments on flat surfaces, with and without pore fluid saturating the pore space. Only by demonstrating that we can produce thermal pressurization weakening reliably can we determine whether or not rough mated surfaces defeat this weakening.

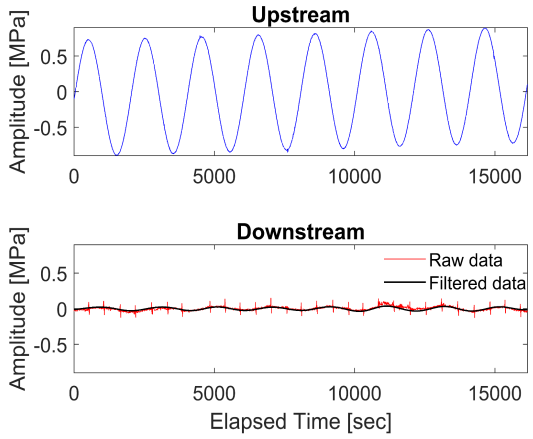

Figure 1. Data showing the phase lag and amplitude reduction between the up- and down-stream ends of a sample during up-stream pressure oscillations in experiment 340pfp.

During this year we have increased our efforts to determine the fluid diffusivity of our samples. In addition to creating a given permeability by our thermal treatment [*Fredrich and Wong*, 1986], the storage capacity of the sample is affected. The ratio of these two determines the thermal diffusivity and this is the important variable for the amount of thermal pressurization. In the past we have measured permeability via a simple Darcy flow technique in which we flow water through the sample. This involves holding the pressure constant on the downstream end of the sample and forcing water into the upstream end at a known rate. However, we have often made this measurement during the initial fluid saturation stage of the experiments with too large a pressure difference between the up- and down-stream ends of the sample. This is inadvisable since permeability depends on the effective pressure, especially if the permeability is due to flat cracks as form during the thermal treatment process we use to create the desired permeability.

Furthermore the storage capacity cannot be determined using the Darcy flow method. Consequently we have begun this year to measure both the permeability and the storage capacity using the pore-pressure oscillation technique [*Bernabe et al.*, 2006; *Fischer*, 1992; *Fischer and Paterson*, 1992; *Kranz et al.*, 1990]. In this method, a small down-stream reservoir is kept at a constant volume while the pressure on the up-stream end of the sample is oscillated sinusoidally in time. The phase shift and the ratio of the up- to down-stream oscillation amplitudes can be used to determine both the permeability and the storage capacity [*Bernabe et al.*, 2006; *Fischer*, 1992; *Fischer and Paterson*, 1992; *Kranz et al.*, 1990]. The raw data from such a measurement is shown in Figure 1.

Changes in friction can occur with large velocity changes in dry samples as well as in fluid saturated ones. We are using diabase with a silica content of only 50 percent in order that weakening due to the presence of thixotropic silica gel does not occur [*Di Toro et al.*, 2003; *Goldsby and Tullis*, 2002; *Roig Silva et al.*, 2004a; b]. In order to contrast the behavior of our fluid saturated samples with those of dry samples, we first show data on the results of large velocity steps on dry samples.

Dry experiments

The dry mechanical behavior of Frederick Diabase was tested under normal and confining stresses of 25 and 20 MPa, respectively, similar to the effective stress conditions of the "wet" experiments. This experimental set was used as a reference for the experiments that were done with pore fluid pressure.

Figure 2 depicts the typical mechanical response of the Frederick Diabase surfaces to a velocity step. Here, the velocity jumps from 3.162 μm/s (reference state velocity) to 2.5 mm/s for 20 seconds. The results show a transient increase in friction at the onset of rapid slip, the friction decreases a bit, but is still higher than when sliding slow (reference state velocity). If we assume that the transient increase in friction scales with the logarithm of the velocity change as in rate and state friction [*Dieterich*, 1979; *Ruina*, 1983], then

$$f = f_0 + a \ln V/V_0 \,, \qquad (1)$$

where f_0 is the friction at the reference state velocity (V_0), a is a proportionality factor and V is the velocity during the velocity step segment.

This velocity-strengthening behavior was observed for a range of sliding velocities, stepping from 1 mm/s to 2.5-7.5 mm/s, which give a-values in the range of 0.008-0.038.

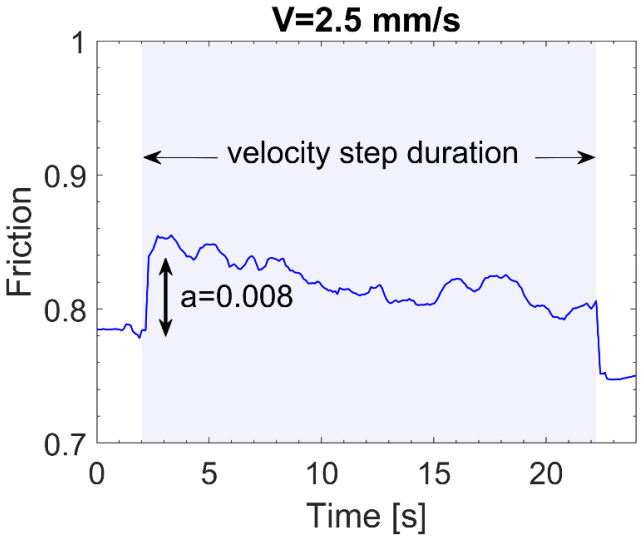

Figure 2. Dry velocity step experiment on a Frederick Diabase surface that had previously been displaced for a total distance of 0.8 m, thus has a fully developed gouge layer (formed through shear). The results indicate that the friction increases transiently with velocity, starting at ~0.78 when sliding at 3.162 μm/s to 0.85 when sliding at 2.5 mm/s. The gray-shaded area in the plot depicts sliding at 2.5 mm/s. Once the velocity is dropped down back to it's original value (unshaded area on the right-hand-side of the plot) the friction decays abruptly.

Pore fluid pressure experiments

These experiments were conducted on water-saturated samples of Frederick Diabase with a set pore pressure. The step velocity experiments with pore fluid pressure were performed on two types of simulated fault zones; (1) Nominally flat bare rock-rock contacts and (2) Gouge filled contacts. The gouge in the second type of experiments was formed through shear sliding of initially bare surfaces for >1 m of total slip. *Beeler et al.* [1996] report approximate constant thickness (70-110 μm) of shear-generated gouge and steady state microstructure for initial bare surfaces of Westerly Granite after ~18 mm of total slip. Thus, we assume that after 1 m of total slip a thick gouge layer has formed in the simulated fault.

Figure 3 depicts the frictional resistance across a bare-surface contact during a velocity step, from steady sliding at 3 μm/s to fast sliding at 2500 μm/s, under a normal stress of 50 MPa, confining pressure of 45 MPa and initial pore pressure (at the onset of rapid slip) of 25 MPa. At slow reference slip-rate the surfaces slide with a friction coefficient of 0.9, once the velocity is increased the friction increases instantaneously before it decays significantly by ~ 40% of its original value. As displacement increases the surfaces regain part of their strength and heal, once the velocity is set to its reference value the surfaces resume steady sliding, albeit at a much lower value of friction ~0.67.

The dashed line in Figure 3 depicts the expected friction for the given velocity step, based on the dry data for initially bare surfaces. The difference between the "dry" (no pore fluid pressure) and "wet" (with fluid pressure) is manifested by the friction coefficient. While it is impossible to get a direct measurement of the pore fluid pressure in the fault zone and still maintain undrained conditions, we can get an estimate based on the changes in friction. By assuming the friction follows the expected model given in equation (1), we can calculate the pore pressure in the fault zone using the effective stress law [*Biot*, 1941; *Terzaghi*, 1923]:

$$f = \frac{\tau}{\sigma - p}, \quad (2)$$

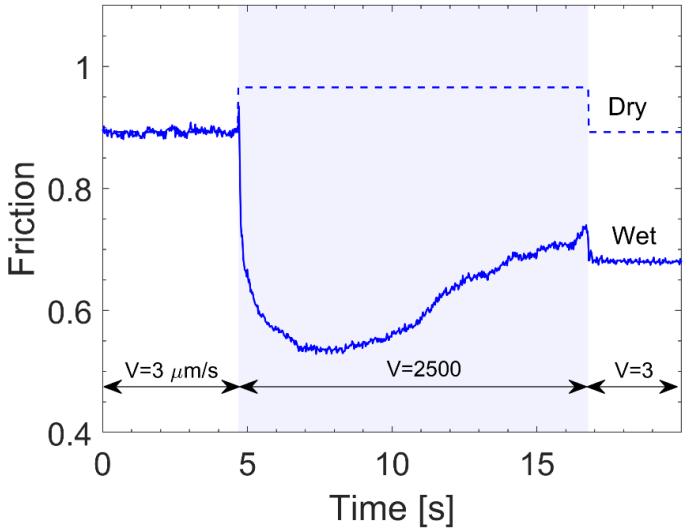

Figure 3. Velocity step experiment on a bare surface contact with pore pressure (solid line) and an expected dry behavior (dashed) for comparison. The shaded area represents the step velocity period (sliding at a rate of 2500 μm/s) while the unshaded areas depict the slow, reference sliding periods (3 μm/s).

where f is the friction coefficient, τ is the shear stress, σ is the normal stress and p is the pore fluid pressure. Substituting equation (2) in (1) and rearranging gives:

$$p = \sigma - \frac{\tau}{f_0 + a \ln \frac{V}{V_0}}. \quad (3)$$

Figure 4 shows the observed shear stress (blue curve) and calculated change in pore fluid pressure (red curve) as a function of slip during the fast slip-rate (2.5 mm/s) part of the experiment. Maximum excess pore fluid pressure (above the controlled initial pressure of 25 MPa) is ~11 MPa, which is reached during the beginning of the fast sliding part. Afterwards, the pore fluid pressure decays (while friction heals) to

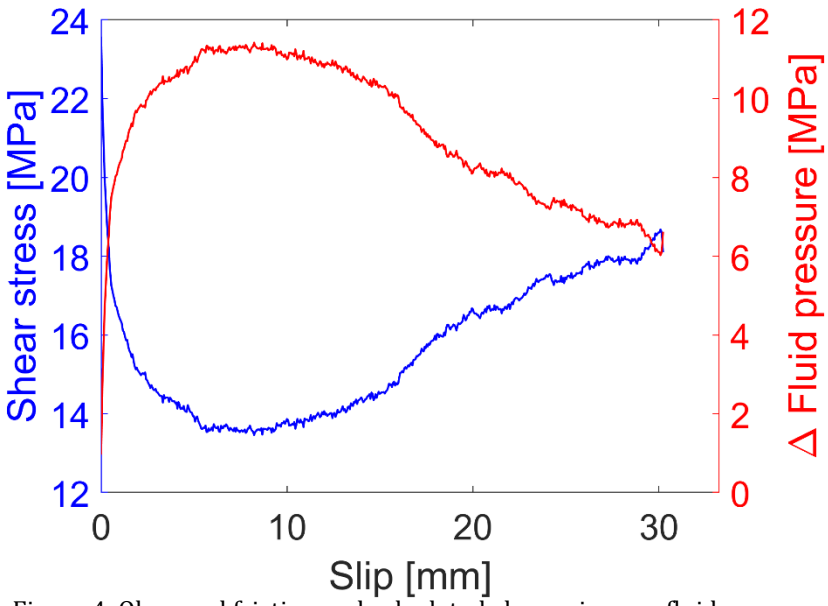

Figure 4. Observed friction and calculated change in pore fluid pressure with slip, during fast sliding at 2.5 mm/s.

about 6 MPa, which corresponds to the lower value of friction, relative to the initial slow-slip steady friction, that was measured after the end of the velocity step (Figure 3). The rapid decay in shear stress (and subsequent increase in calculated pore fluid pressure) at the beginning of the velocity step (first ~8 mm of slip, Figure 4) implies efficient heating and pressurization of the pore fluids present in the fault zone. Later, with continued slip, the surfaces regain some of their inherent strength, which may suggest that pressurization is progressively diminishing. This is not the only experiment in which we see this and we do not presently understand it. Our current speculation is that it is somehow due to changes in the fluid diffusivity, and perhaps of the undrained pressurization factor Λ [*Rice*, 2006], as a function of effective pressure, which varies spatially and temporally in the sample. We are working on modeling this possibility with FEM.

When we look at a succession of velocity steps, of the same sample, we can see similar mechanical behavior as observed in Figure 3, but with smaller drops in friction and regaining of friction to a level close to the predicted dry behavior (Figure 5). The drops in friction become progressively smaller with each run, while at the end of each fast part (in each run) the friction returns to its initial value before the velocity step. These results imply that pressurization is efficient for smaller and smaller time windows, and perhaps hydraulic diffusivity is too high to maintain ongoing dynamic weakening. This argument is further supported by the almost identical friction before and after each velocity step. This progressive change with total displacement could result from progressive damage to the near-fault volume of the diabase sample. We do not yet have petrographic thin sections from the samples to help evaluate this hypothesis.

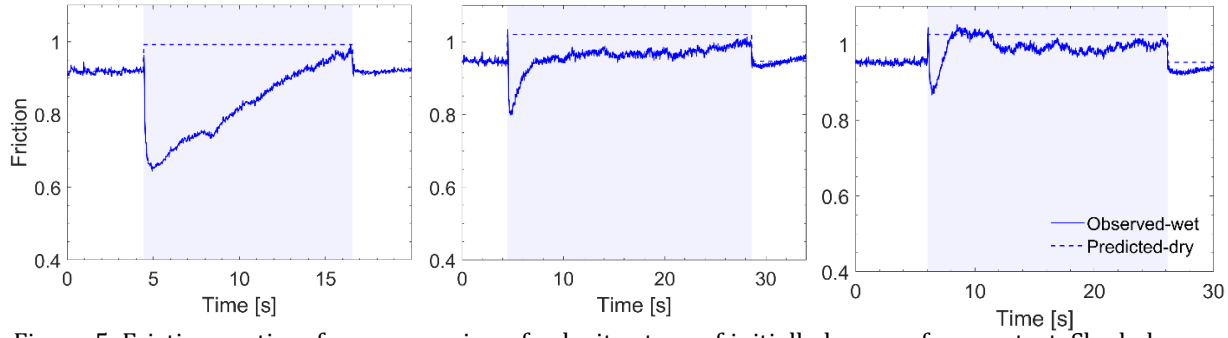

Figure 5. Friction vs. time for a succession of velocity steps of initially bare surface contact. Shaded areas are fast slip-rate (2.5 mm/s) parts, unshaded areas are the reference velocity (3 μm/s) parts. The predicted (equation (1)) friction is plotted (dashed lines) for comparison.

Gouge with pore fluid pressure experiments

Another type of experimental fault zones started initially as nominally flat, bare surfaces, but slid further, at least 1 m, and consequently developed a layer of generated gouge, perhaps 50-200 mm thick.

Figure 6 plots the results from two runs on the same sample, each at a different velocity (during the velocity step part – shaded areas). The experiment was performed under a normal stress of 50 MPa, confining pressure of 49 MPa and pore pressure of 25 MPa. The two results demonstrate a transient increase in friction at the onset of fast sliding and then a significant decay in friction (~40%) with continued fast slip. The weakening rate decreases as the sliding continues until, at least for the faster run (Figure 6 – right) some increase in friction is observed. This weakening behavior is in stark contrast to the predicted dry behavior of this type of faults, based on earlier observations.

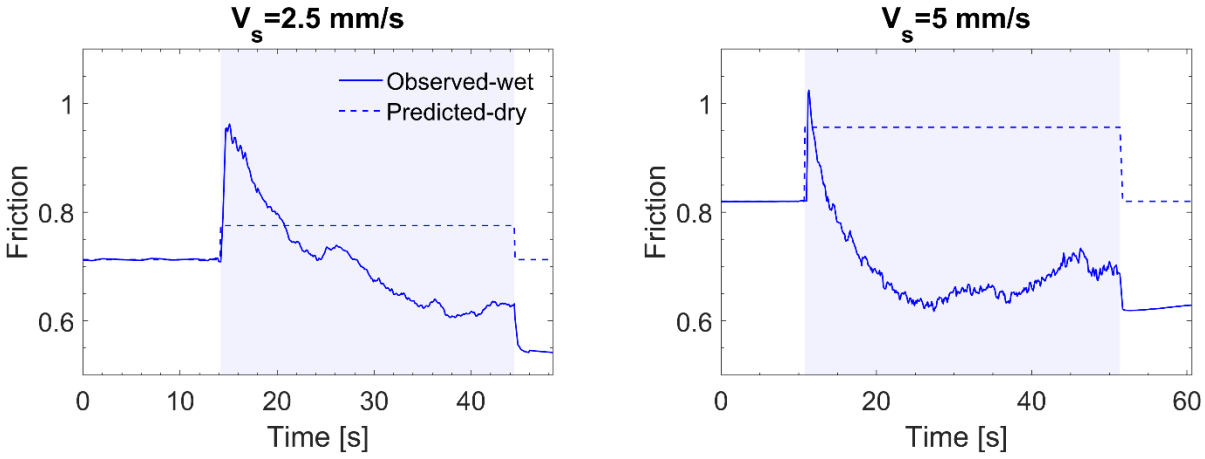

Figure 6. Velocity step experiment results for gouge filled interface. The solid curve is the observed friction during the experiment, whereas the dashed curves are the predicted, dry friction based on the model presented by equation (2). The shaded area represents the fast-slip step duration (Left – $slip\ rate = 2.5\ mm/s$; Right – $slip\ rate = 5\ mm/s$), and the unshaded area represents the reference velocity ($1\ \mu m/s$).

The gouge experiment results follow the [*Rice*, 2006] thermal pressurization weakening model quite well if the weakening is observed for the full duration of the velocity step. An example can be seen in Figure 7, where the results of a non-linear least squares algorithm with modelled parameters (from the *Rice* [2006] model), decay distance (L^*) and initial pore pressure (p_0) are fitted for. In this case, $p_0 = 19\ MPa$ and $L^* = 296\ mm$.

The inferred pore pressure at the onset of fast sliding (p_0) is slightly smaller than the set pore pressure of 25 MPa. This instantaneous decrease in fluid pressure, which conforms with a large transient increase in friction (Figure 6), much higher than the dry, direct effect frictional transient (**Error! Reference source not found.**), may be a product of transient dilatancy hardening [*Brace and Martin*, 1968], which is observed using our internal axial displacement transducer.

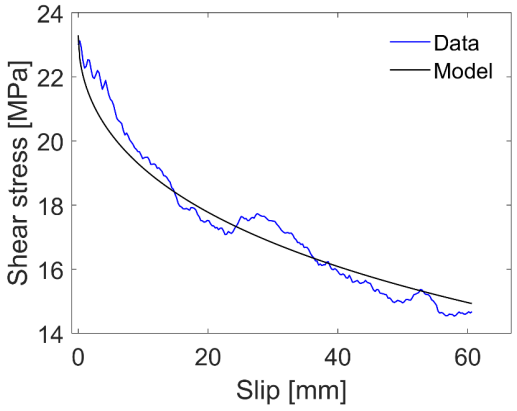

Figure 7. Shear stress vs. slip for a fast slip-rate velocity step in gouge fault. The model (black curve) agrees with the data (blue curve) for the full duration of the velocity step (60 mm of slip).

C. References Cited

Andrews, D. J. (2002), A fault constitutive relation accounting for thermal pressurization of pore fluid, *J. Geophys. Res.*, *107*, 12.

Beeler, N. M., T. E. Tullis, M. L. Blanpied, and J. D. Weeks (1996), Frictional behavior of large displacement experimental faults, *J. Geophys. Res.*, *101*, 8697-8715.

Bernabe, Y., U. Mok, and B. Evans (2006), A note on the oscillating flow method for measuring rock permeability, *Int. J. Rock Mech. Min. Sci.*, *43*, 311-316.

Biot, M. A., . (1941), General theory of three-dimensional consolidation, *J. Appl. Phys.*, *12*, 155.

Bizzarri, A., and M. Cocco (2006a), A thermal pressurization model for the spontaneous dynamic rupture propagation on a three-dimensional fault: 1. Methodological approach, *J. Geophys. Res.*, *111*, B05303, doi:05310.01029/02005JB003862.

Bizzarri, A., and M. Cocco (2006b), A thermal pressurization model for the spontaneous dynamic rupture propagation on a three-dimensional fault: 2. Traction evolution and dynamic parameters, *J. Geophys. Res.*, *111*, B05304, doi:05310.01029/02005JB003864.

Brace, W. F., and R. J. Martin Iii (1968), A test of the law of effective stress for crystalline rocks of low porosity, *International Journal of Rock Mechanics and Mining Sciences & Geomechanics Abstracts 5*(5), 415-426.

Di Toro, G., D. L. Goldsby, and T. E. Tullis (2003), Friction falls to zero at seismic slip rates, *Eos. Trans. Am. Geophys. Union*, *84*(46), Fall Meeting Suppl., Abstract S41B-02.

Dieterich, J. H. (1979), Modeling of rock friction, 1, Experimental results and constitutive equations, *J. Geophys. Res.*, *84*, 2161-2168.

Fischer, G. J. (1992), The determination of permeability and storage capacity: pore pressure oscillation method, in *Fault mechanics and transport properties of rocks*, edited by B. Evans and T.-f. Wong, pp. 187-211, Academic Press, New York.

Fischer, G. J., and M. S. Paterson (1992), Measurements of permeabiity and storage capacity in rocks during deformation at high temperature and pressure, in *Fault mechcanics and transport properties of rocks*, edited by B. Evans and T.-f. Wong, pp. 213-251, Academic Press, New York.

Goldsby, D. L., and T. E. Tullis (2002), Low frictional strength of quartz rocks at subseismic slip rates, *Geophys. Res. Lett.*, *29*(17), 1844, doi:1810.1029/2002GL015240.

Kranz, R. L., J. S. Saltzman, and J. D. Blacic (1990), Hydraulic diffusivity measurements on laboratory samples using an oscillating pore pressure method, *Int. J. Rock Mech. Min. Sci.*, *27*, 345-352.

Lachenbruch, A. H. (1980), Frictional heating, fluid pressure, and the resistance to fault motion, *J. Geophys. Res.*, *85*, 6249-6272.

Lapusta, N., and J. R. Rice (2004a), Earthquake sequences on rate and state faults with strong dynamic weakening, paper presented at 2004 SCEC Annual Meeting Proceedings and Abstracts, Southern California Earthquake Center, PalmSprings, California, 2004.

Lapusta, N., and J. R. Rice (2004b), Earthquake sequences on rate and state faults with strong dynamic weakening, *Eos. Trans. Am. Geophys. Union, Fall Meeting Suppl.*, *85*(47), T22A-05.

Lee, T. C., and P. T. Delaney (1987), Frictional Heating and Pore Pressure Rise Due to a Fault Slip, *Geophysical Journal of the Royal Astronomical Society*, *88*(3), 569-591.

Mase, C. W., and L. Smith (1985), Pore-fluid pressures and frictional heating on a fault surface, *Pure Appl. Geophys.*, *122*, 583-607.

Mase, C. W., and L. Smith (1987), Effects of frictional heating on the thermal hydrologic and mechanical response of a fault, *J. Geophys. Res.*, *92*, 6249-6272.

Noda, H. (2008), Frictional constitutive law at intermediate slip rates accounting for flash heating and thermally activated slip process, *J. Geophys. Res.*, doi:10.1029/2007JB005406.

Noda, H., E. M. Dunham, and J. R. Rice (2009), Earthquake ruptures with thermal weakening and the operation of major faults at low overall stress levels, *J. Geophys. Res.*, *114 (B07302)*, doi:10.1029/2008JB006143.

Noda, H., and N. Lapusta (2010), Three-dimensional earthquake sequence simulations with evolving temperature and pore pressure due to shear heating: Effect of heterogeneous hydraulic diffusivity, *J. Geophys. Res.*, *115*, B12314.

Noda, H., and T. Shimamoto (2005), Thermal pressurization and slip-weakening distance of a fault: An example of the Hanaore fault, southwest Japan, *Bull. Seis. Soc. Am.*, *95*(4), 1224-1233.

Rempel, A. W., and J. R. Rice (2006), Thermal pressurization and onset of melting in fault zones, *Journal of Geophysical Research-Solid Earth*, *111*(B9), B09314, doi:09310.01029/02006JB004314.

Rice, J. R. (2006), Heating and weakening of faults during earthquake slip, *Journal of Geophysical Research-Solid Earth*, *111*(B5), doi:10.1029/2005JB004006.

Rice, J. R., and M. Cocco (2007), Seismic fault rheology and earthquake dynamics, in *The Dynamics of Fault Zones*, edited by M. R. Handy, p. in press, MIT Press, Cambridge, Mass.

Rice, J. R., E. M. Dunham, and H. Noda (2010), Thermo- and hydro-mechanical processes along faults during rapid slip, in *Meso-Scale Shear Physics in Earthquake and Landslide Mechanics*, edited by Y. Hatzor, J. Sulem and I. Vardoulakis, pp. 3-16, CRC Press.

Roig Silva, C., D. L. Goldsby, G. Di Toro, and T. E. Tullis (2004a), The role of silica content in dynamic fault weakening due to gel lubrication, paper presented at 2004 SCEC Annual Meeting Proceedings and Abstracts, Southern California Earthquake Center, Palm Springs, California.

Roig Silva, C., D. L. Goldsby, G. Di Toro, and T. E. Tullis (2004b), The role of silica content in dynamic fault weakening due to gel lubrication, *Eos. Trans. Am. Geophys. Union, Fall Meeting Suppl.*, *85*(47), T21D-07.

Ruina, A. L. (1983), Slip instability and state variable friction laws, *J. Geophys. Res.*, *88*, 10359-10370.

Schmitt, S. V., and P. Segall (2009), Thermal pressurization during "slip law" frictional earthquake nucleation, *Poster, 2009 SCEC Annual Meeting*.

Segall, P., and J. R. Rice (2006), Does shear heating of pore fluid contribute to earthquake nucleation?, *Journal of Geophysical Research-Solid Earth*, *111 (B09316)*, doi:10.1029/2005JB004129.

Sibson, R. H. (1973), Interactions between temperature and fluid pressure during earthquake faulting - A mechanism for partial or total stress relief, *Nature*, *243*, 66-68.

Terzaghi, K. V. (1923), Die Berechnung der Durchas- sigkeitsziffer des Tones aus dem Veriauf der hydrodynamischen Spannungserscheinungen, *Sitzungsber. Akad. Wiss. Wien Math Naturwiss*, *K1*(Abt. 2A, 132), 105.